Shaoyang Dong · Yusheng Jiang · Xiong Yu

Analyses of the Impacts of Climate Change and Forest Fire on Cold Region Slopes Stability by Random Finite Element Method

Abstract Increasing number of landslides occurred in the cold regions over the past decades due to rising temperature or forest fires associated with climate change. The instability of thawing slopes caused serious damages to transportation infrastructure, residential properties, and losses of human lives. These types of landslides, however, are difficult to analyze by the traditional limit equilibrium methods due to the coupled thermos-hydro-mechanical multiphysics processes involved. This paper describes a novel microstructure-based random finite element model (RFEM) to simulate the stability of permafrost slope subjected to climate change, including the increasing extent of thawing by warm atmosphere and thermal load due to forest fire. The properties of frozen soil are captured with random finite element model incorporating soil-phase coding. The thermomechanical responses of a permafrost slope are simulated to obtain the temperature, displacement, and stress fields. From these, the local factors of safety are obtained, which predict failure slumps along the slope that are consistent with the field-observed failure behaviors in permafrost slopes. The effects of climate change on the permafrost slope stability are analyzed for the years of 1956, 2017, and 2045. The results demonstrated appreciable amount of effects of climate change on the extent of slope failure zones. Forest fire led to melting of frozen soil and also affects the slope stability primarily in the shallow depth.

Keywords Slope stability · Random finite element model · Climate change · Forest fire

Introduction

In the recent decades, the northern hemisphere regions with permafrost soils and seasonally frozen ground have experienced significant warming trends due to the climate change (Frauenfeld et al. 2007; Zwiers 2002; Sturm et al. 2001; Alley et al. 2003). High altitude and high latitude areas such as the Alps in Europe, Qinghai-Tibet Plateau in China, northern Canada, Russia, and Alaska have observed accelerated degradation rate of permafrost and seasonally frozen soil (Haeberli and Beniston 1998; Shaoling et al. 2000; Thibault and Payette 2009; Jorgenson et al. 2001; Luo et al. 2019; Niu et al. 2016). In addition, melting of frozen soil caused by forest fire has triggered landslides, mudflows, and rock falls in cold regions. These geological disasters have reshaped the landscape, destroyed the local transportation infrastructures, and even caused huge losses to human lives and properties (Davies et al. 2001; Harris et al. 2001; Wang et al. 2014; Gruber et al. 2004; Kim et al. 2015; Bo et al. 2008; Gruber and Haeberli 2007).

Slope stability analyses are generally performed by the conventional limit equilibrium methods (Bishop 1955; Janbu 1973; Morgenstern and Price 1965; Duncan 1996). These methods have been applied extensively for the general slope stability analyses in the engineering practice. Some of the limit equilibrium methods assume a circular slope failure curve where sliding zones are divided into slices, although stability can also be analyzed with non-circular failure curves or no discretization into slices. Abiding the equilibrium of force and equilibrium of momentum on each slice, the factor of safety FS is generally determined as that the soil strength parameters reduced by FS lead to equilibrium conditions (i.e., the mobilized shear strength in equilibrium with the total shear stress) along the prescribed failure curve. The limit equilibrium methods, however, may not be effective to analyze the stability of thawing slopes. Because from documented field studies, the failure of thawing slope was observed to occur in parallel to the slope surface, similar to an infinite slope. This is different from commonly observed landslides with curved sliding surfaces (Davies et al. 2001; Wang et al. 2014; Morgenstern and Price 1965; Duncan 1996; Wu 1984; McRoberts and Morgenstern 1974). The thaw slumping along permafrost slope is less thick compared with commonly observed failure zone along regular slopes. The thickness of slump is determined by the soil temperature and the thawing depth. Therefore, the limit equilibrium methods provide little insight into the location of the failure surface along a thawing slope. To overcome this limitation, the methods of local factor of safety (LFS) and random finite element are combined together to simulate the stability of thawing slopes (Lu et al. 2012; Dong and Yu 2016; Dong and Yu 2017; Dong and Yu 2018). The LFS of slope is defined as the ratio of the local shear strength to the local shear stress of a particular element in the slope. LFS is a scalar field, a function of position in the slope. The random finite element method adds randomness to characterize the inherent variabilities of soil and geological features, which is improvement over the traditional finite element method (Fenton and Griffiths 2003; Griffiths et al. 2006; Griffiths et al. 2010; Fenton et al. 2005). As generally known, frozen soil is a four-phase material that contains solid particles, ice, water, and air. These phases have their corresponding mechanical and thermal properties (such as Young's modulus, Poisson's ratio, density, thermal conductivity, heat capacity, coefficient of thermal expansion) and are randomly distributed in the thawing slope. The LFS determined by the random finite element method allows to trace the stress state and development process of failure surface along the thawing slope.

This paper describes the development and implementation of a novel random finite element model (FREM) to analyze the stability of sequentially thawing slopes. The RFEM captures the spatial randomness of soil parameters via phase coding. With the RFEM model, the mechanical parameters of both frozen soil and unfrozen soil are simulated and calibrated by the
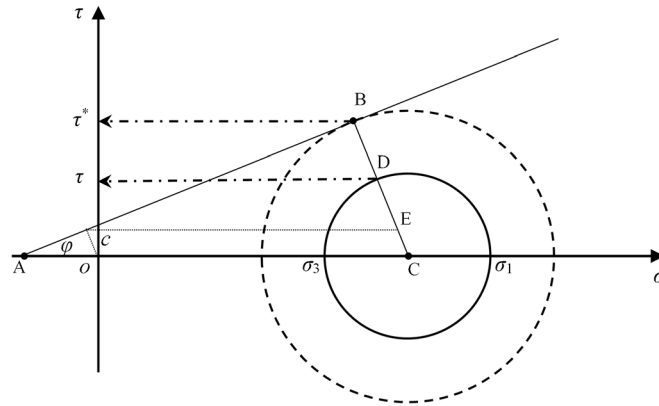
Fig. 1 Illustration of local factor of safety from Mohr circles

experimental data. With the calibrated soil model, the responses of a permafrost slope to annual climatic temperature process are simulated with the RFEM. From this, the slope deformation and the local factor of safety distribution along the slope are obtained. The effects of burning along the slope on the slope stability are also simulated and analyzed. The results unveil the important impacts of climate change on the stability of slope in the cold region.

Theoretical background

Local factor of safety

The local factor of safety (LFS) is defined based on the comparison of the local stress condition to the soil strength. As illustrated in Fig. 1, the solid Mohr circle describes the actual stress condition at a location in the slope. The factor of safety is defined as the ratio of the distance of stress centroid to the strength curve (CB) to the radius of the Mohr circle (CD) (Fig. 1). The corresponding mathematical relationship is given in Eq. (1).

$$
\begin{aligned}
\text{LFS}(x,y) &= \frac{\tau^*(x,y)}{\tau(x,y)} = \frac{|\text{BC}|}{|\text{DC}|} = \frac{|\text{BE}| + |\text{EC}|}{|\text{DC}|} \\
&= \frac{\dfrac{\sigma_1 + \sigma_3}{2}\sin\phi + c\cdot\cos\phi}{\dfrac{\sigma_1 - \sigma_3}{2}}
\end{aligned}
\tag{1}
$$

where c and ϕ are cohesion and the angle of internal friction, respectively, of frozen or unfrozen soils (depending upon the thermal condition). They are also called shear strength parameters of soils. σ_1 and σ_3 are the maximum and minimum principal stress of soils, respectively, which can be obtained from the finite element analyses.

The stress state at any point in the slope corresponds to shear stress τ and has a shear strength τ^*. The ratio of shear strength to shear stress is defined as the local factor of safety (LFS), which indicates how far the current shear stress state is
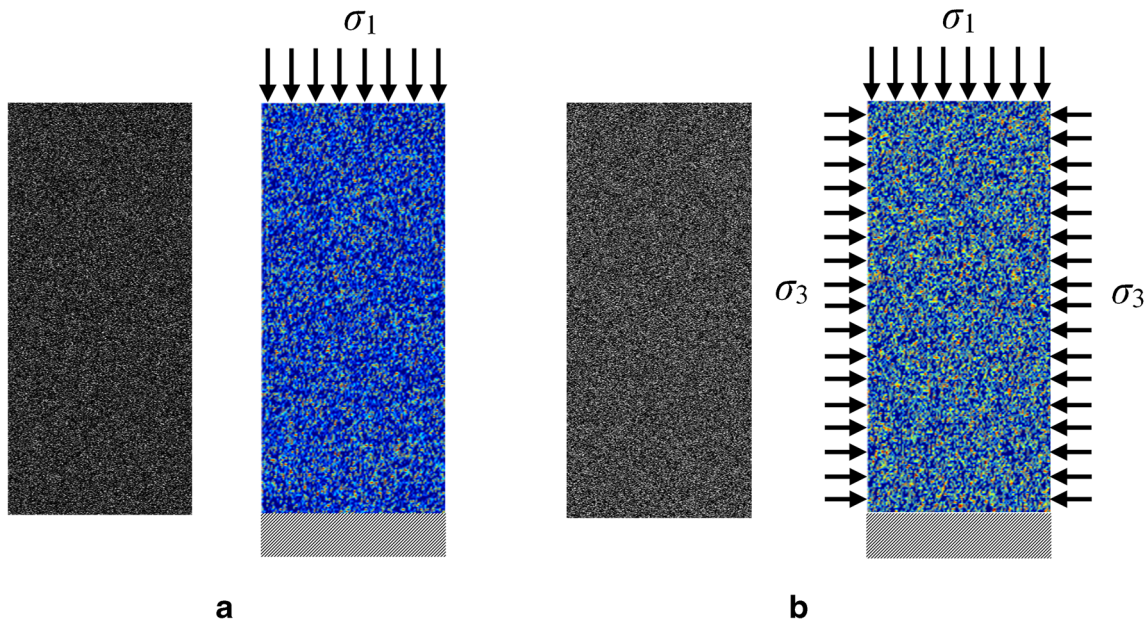

Fig. 2 a RFEM phase-coded model for uniaxial test of frozen soil. **b** RFEM phase-coded model for triaxial test of unfrozen soil. The gray-scale image is generated from MATLAB and the color image is the converted version from COMSOL

Table 1 Physical and measured mechanical properties of frozen and unfrozen soil specimens

Constant	Value	Units	Description
R	1.65	cm	Radius of soil specimen
H	7.2	cm	Height of soil specimen
w_o	0.15	1	Initial water content
ρ	1708	kg/m^3	Dry density of soil specimen
G_s	2.65	1	Specific gravity of soil specimen
E_{frozen}	20	MPa	Young's modulus of frozen soil specimen
$E_{unfrozen}$	10.2	MPa	Young's modulus of unfrozen soil specimen
$\sigma_{c,frozen}$	775	kPa	Unconfined compressive strength of frozen soil specimen
$\sigma_{c,unfrozen}$	375	kPa	Unconfined compressive strength of unfrozen soil specimen

from failure. As illustrated in Fig. 1, if Mohr circle is separate from the Mohr-Coulomb failure envelope, τ^*/τ is greater than 1, which indicates that the point in the slope is currently stable. If the Mohr-Coulomb failure envelope is tangent or intersects with Mohr circle, τ^*/τ is less than or equal to 1, and the point in the slope is unstable.

The value of LFS is a scalar function dependent upon the stress conditions at a particular location and is an indicator on the stability of each location in the slope. The contour of LFS gives the areas that have the similar likelihood of failure.

The local factor of safety in thawing slopes is not only a scalar function of position, but also a function of time and temperature. For example, during the thawing process, the shear strength of the soil would decrease and it is affected by the temperature (Hivon and Sego 1995; Nixon and Lem 1984; Chamberlain et al. 1972; Arenson and Springman 2005; Czurda and Hohmann 1997). On the other hand, the internal stress in the slope would increase during the freezing process due to matric suction and ice expansion. The local factor of safety has the advantages of providing the location of initial failure and allows describing how the region of instability evolves with time and temperature.

## Determination of shear strength parameters for frozen and unfrozen soils

Preparation of physical and digital soil specimens

In order to determine the local factor of safety and analyze the stability of thawing slope, the information of shear strength parameters (cohesion and the angle of internal friction) of frozen and unfrozen soils is needed. Combined experiments and random finite element model (RFEM) simulations are used to determine the soil strength parameters. The physical soil specimens of silty clay are compacted by Harvard miniature compactor with soil particles and water uniformly distributed. The extruded soil specimens were subjected to freezing conditions and mechanical loads by unconfined compression test. In the meanwhile, the corresponding digital soil specimens are prepared by RFEM to simulate the behaviors of the frozen/unfrozen soils. The volume portions of different phases are incorporated in producing the RFEM model based on the physical properties of the soil specimen prepared by Harvard miniature compactor.

The following steps are undertaken to simulate the phase distribution and microstructure of frozen soils: (1) determination of volume content of different phases. The volumetric
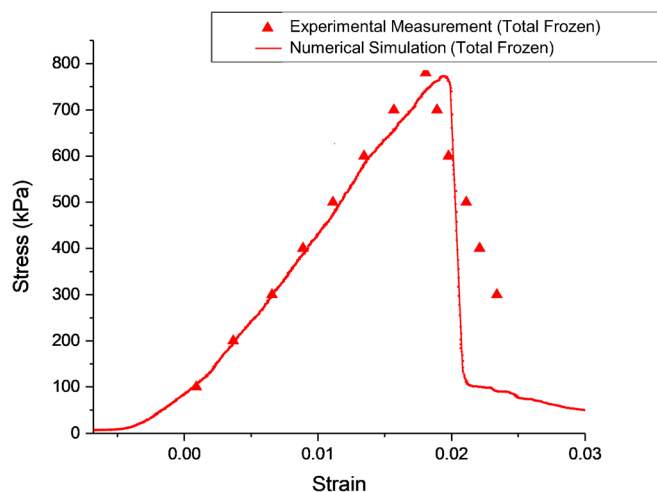
Fig. 3 Comparison of the stress-strain curve of a completely frozen soil specimen by experimental measurement versus numerical simulation with RFEM
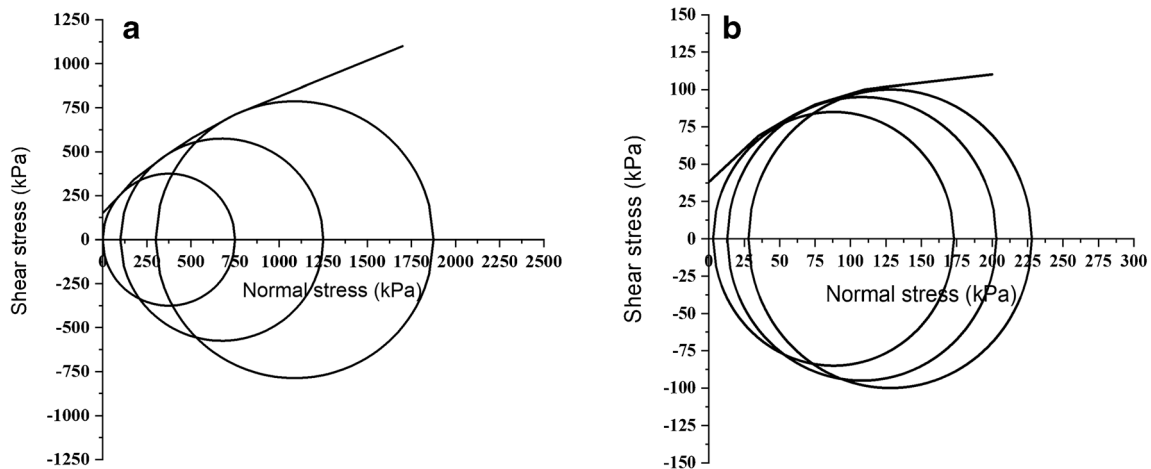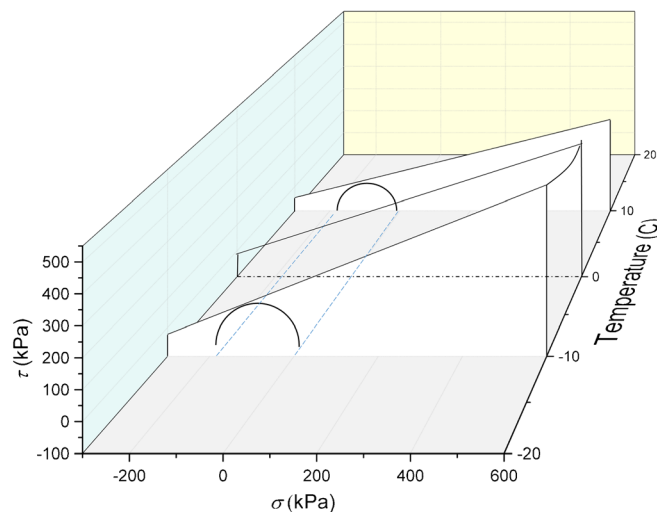
Fig. 4 Mohr circles and the Mohr-Coulomb failure envelopes from RFEM simulations of soil specimens subjected to triaxial tests for **a** frozen soil and **b** unfrozen soil

content of each phase is calculated from the physical information including the dry density, water content, porosity, and specific gravity. (2) Generation of digital matrix for virtual soil specimen. A $m \times n$ matrix is generated by use of MATLAB, where each cell in the matrix contains the corresponding phase coding. For the dimension of the matrix, m is set to be equal to the height of the soil specimens divided by the average diameter of the soil particle, while n equals to the radius of the soil specimens divided by the average diameter of the soil particle. Thus, $m \times n$ equals the total number of elements in the image of a 2D soil model specimen. (3) Phase coding of digital soil specimen. Each element in the matrix is assigned with a value to represent a particular phase of the soil specimens. Four different numbers (0, 1/3, 2/3, and 1) are assigned to represent different phases (soil particles, water, ice, and air) respective within the soil specimens. The phase is determined by a random number generator where the probability of occurrence of a particular phase is determined by the volumetric content of that phase. For the four-phase soil specimen, the phase value protocol is set to 0, 1/3, 2/3, 1 for soil particle, ice, water, and air respectively. This process was repeated for each pixel element of

the m by n matrix. Consequently, the m by n matrix contains the phase coding that represents the volume proportion of different phases, which can be visually shown as a gray-scale image. With the procedure described, the probability of occurrence or the percentage of each phase is approximately equal to the volumetric content of each phase when the m by n matrix is sufficiently large. The 2D phase-coded frozen and unfrozen soil models generated from MATLAB are converted into COMSOL. COMSOL is a finite element software that supports importing images and assigning material properties based on the color scale of the image. The phase is color coded in COMSOL with dark blue, light blue, yellow, and red to represent soil particles, ice, water, and air, respectively (Fig. 2a and b). The responses of digital soil specimen to the uniaxial test (Fig. 2a) and triaxial test (Fig. 2b) can then be studied by applying proper load and boundary conditions.
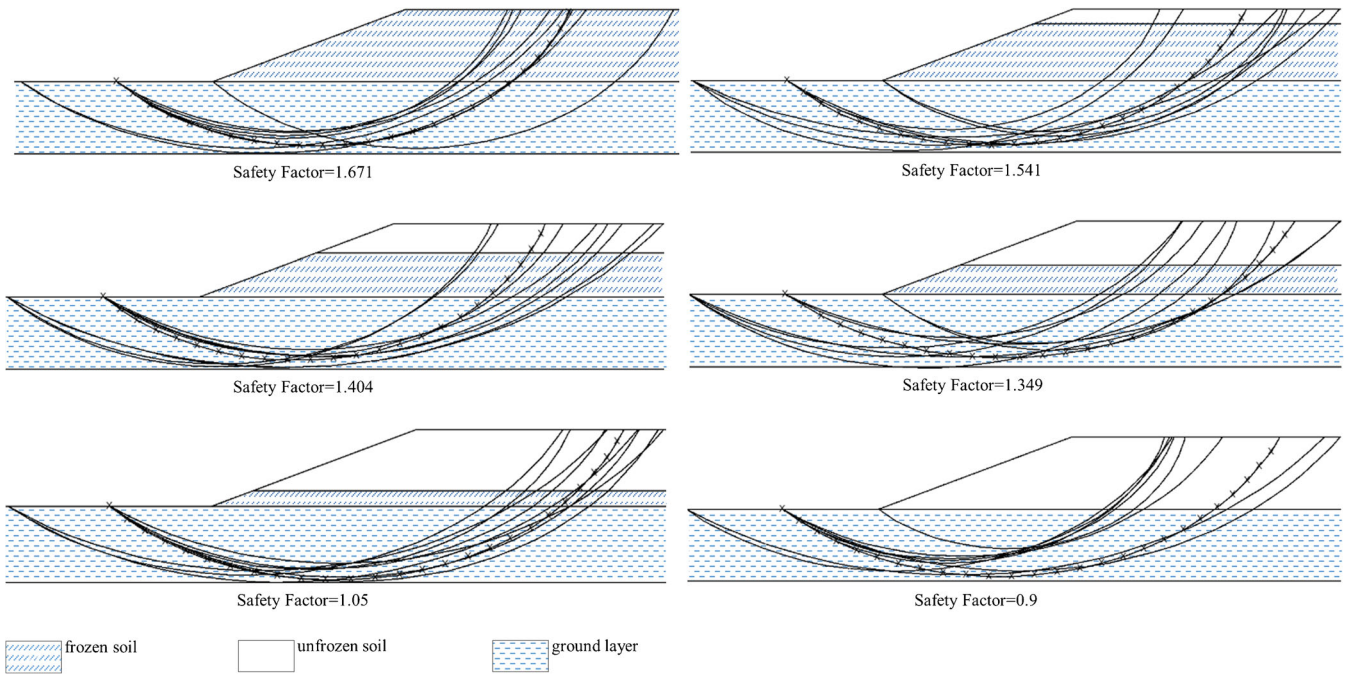
Calibration of the mechanical property parameters of soil phases
The parameters of soil phases (particularly soil solids and ice) are calibrated by comparison of the experimental results and RFEM simulations under the corresponding stress conditions. Firstly, the

Fig. 5 Illustration of the failure of Mohr circle from frozen state to thawed state

Safety Factor=1.671

Safety Factor=1.541

Safety Factor=1.404

Safety Factor=1.349

Safety Factor=1.05

Safety Factor=0.9

frozen soil · unfrozen soil · ground layer

Fig. 6 The stability of thawing slope at different extents of thawing calculated by simplified Bishop method

uniaxial compressive test was conducted to obtain the Young's modulus and compressive strength of complete frozen or complete unfrozen soil specimens. The results are summarized in Table 1.

Random finite element models were then generated based on the phase composition of the physical soil specimens and were applied to simulate the responses of the digital specimen under uniaxial compression test. The fixed constraint is applied at the bottom of the phase-coded frozen soil model and the pressure load σ_1 is applied on the top of the model. The mechanical parameters are assigned to each pixel based on phase coding of the image. By comparing the simulated stress-strain curve with the experimental curve (Fig. 3), the mechanical parameters of each phase in frozen/unfrozen soils (i.e., the mechanical properties of soil solid and ice phases) were obtained by calibration against the mechanical experiments (Table 1).

Prediction of the strength of unfrozen soil

With the calibrated parameters, random finite element simulation (RFEM) was conducted to simulate the triaxial experiments on frozen/unfrozen soil specimens under different confining pressures. The calibrated parameters are assigned to each pixel based on the color scale of the image. As shown in Fig. 2b, the fixed constraint is applied at the bottom of the unfrozen soil model. The confining pressure σ_3 and the compressive pressure σ_1 are exerted on sides and on top of the soil model, respectively. The deviatory stress increases until the simulation becomes numerically unstable, which is used to indicate failure. The stress condition at failure is recorded and analyzed. The simulations were repeated for different magnitudes of confining pressures. The Mohr-Coulomb failure envelope and the shear strength parameters were obtained from stress conditions corresponding to the failure conditions based on the simulation results.

The simulated Mohr circles and the Mohr-Coulomb failure envelopes for frozen soil and unfrozen soil are plotted in Fig. 4. From the Mohr-Coulomb failure envelopes, the shear strength parameters corresponding to linear fitting can be determined. For the frozen soil, cohesion and the angle of internal friction are determined to be 150 kPa and 30°, respectively. For the unfrozen soil, cohesion and the angle of internal friction are 37 kPa and 20°, respectively. The simulation results indicate that both shear strength parameters, c and ϕ, decrease when frozen soil thaws (Fig. 5), which is consistent with observations from prior research and engineering practice (McRoberts and Morgenstern 1974; Wang et al. 2007). This demonstrates the dependency of soil shear strength parameters on temperature, which is schematically illustrated in Fig. 5. As temperature decreases from above 0 °C to below 0 °C, both the shear strength parameters increase abruptly.

Stability of thawing slope in cold region

The height of the slope is assumed to be 4.5 m with slope gradient of 1:2. The soil in the slope is assumed to be the same soil used in the experiment and RFEM numerical simulation with physical and mechanical properties are listed in Table 1. The slope is assumed to be totally frozen and then subjected to thawing conditions.

Analyses by simplified Bishop's method

The simplified Bishop method is one of the popular limit equilibrium methods for slope stability analyses. The slope is divided into five horizontal layers with heights for the convenience of describing different thawing depths. The slope is assumed to be thawed gradually from top layer to the bottom layer by sequentially replacing the strength parameters of corresponding layer of frozen soil with that of the unfrozen soil.

Table 2 Constant parameters for RFEM simulation of thawing slopes

Constant	Value	Units	Description
W	15	m	Horizontal distance of the study region
H	4.5	m	Height of the slope
SR	1:2	1	Slope ratio
w_o	0.15	1	Initial water content
ρ	1708	kg/m^3	Dry density of soil specimen
d	50	μm	Diameter of soil particle
Gs	2.65	1	Specific gravity of soil specimen
E_s	10.2	GPa	Young's modulus of soil particle
E_i	9	GPa	Young's modulus of ice
E_w	3.9×10^{-5}	Pa	Young's modulus of water
E_a	0	Pa	Young's modulus of air
μ_s	0.3	1	Poisson's ratio of soil particle
μ_i	0.3	1	Poisson's ratio of ice
μ_w	0.5	1	Poisson's ratio of water
μ_a	0	1	Poisson's ratio of air
ρ_s	2600	kg/m^3	Density of soil particle
ρ_i	917	kg/m^3	Density of ice
ρ_w	1000	kg/m^3	Density of water
ρ_a	1.29	kg/m^3	Density of air
k_s	2	W/m·K	Thermal conductivity of soil particle
k_i	2.2	W/m·K	Thermal conductivity of ice
k_w	0.58	W/m·K	Thermal conductivity of water
k_a	0.025	W/m·K	Thermal conductivity of air
Cp_s	835	J/kg·K	Heat capacity of soil particle
Cp_i	1960	J/kg·K	Heat capacity of ice
Cp_w	4181.3	J/kg·K	Heat capacity of water
Cp_a	1005	J/kg·K	Heat capacity of air
L_f	334	kJ/kg	Latent heat fusion of water
α_s	9×10^{-6}	1/K	Volumetric coefficient of thermal expansion of soil particle
α_i	1.9×10^{-4}	1/K	Volumetric coefficient of thermal expansion of ice
α_w	2.07×10^{-4}	1/K	Volumetric coefficient of thermal expansion of water
α_a	3.43×10^{-3}	1/K	Volumetric coefficient of thermal expansion of air

The calculation results of global factor of safety at different extent of thawing by the simplified Bishop method are shown in Fig. 6. As seen from this figure, the slope is most stable under the complete frozen condition with a safety factor of 1.671. The factor of safety (FS) continuously decreases during the thawing process. The FS at the totally thawed state is 0.9 which indicates slope failure.

This simplified case indicates that shear strength parameter plays an important role in determining the safety factor and the stability of the slope. The thawing slope gradually lost its stability due to the reduction of the shear strength when frozen soil melted to unfrozen soil. This method, however, has some drawbacks analyzing the stability of thawing slopes. Firstly, it is assumed that the failure surface of the thawing slope is circular with the location of the circular surface predetermined. For most thawing slopes in the reality, however, the failure surface is not circular. Secondly, the deformation of the thawing slope and the failure surface is affected by the temperature distribution inside the slope, which is not considered in the conventional slope stability analyses. Therefore, new analyses methods and simulation tools are necessary to holistically simulate the stability of thawing slopes.
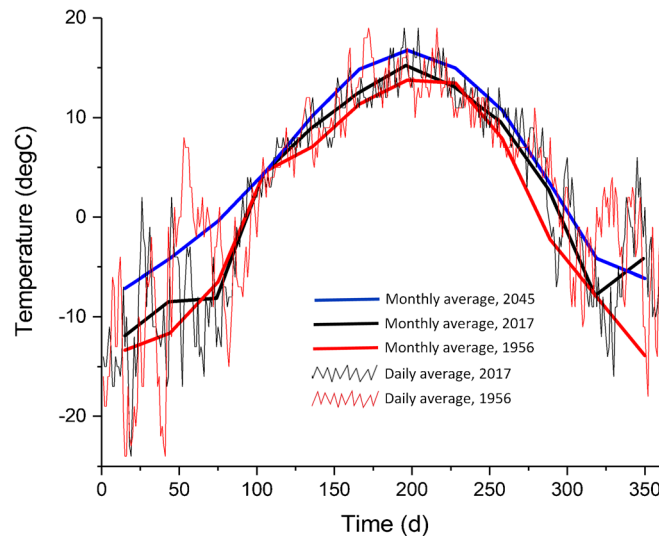
Fig. 7 The average daily (1956 and 2017) and monthly (1956, 2017, and 2045) temperatures at Anchorage, Alaska (the average monthly temperatures in 2045 at Anchorage, Alaska, are referenced from: https://alaskamastergardener.community.uaf.edu/2018/10/13/mountainside-gardening/ (checked on Dec 30, 2020)

## Stability of thawing slope by random finite element method

As a special type of finite element model, the random finite element (RFEM) method holistically captures the thermal heat transfer and mechanical weakening in thawing slope. The randomness captures the effects of the physical constituents of soils on the thermal and mechanical behaviors. The RFEM simulation method combined with the local factor of safety concept allows to simulate the stability of thawing slope subjected to climate conditions. It aims to illustrate the effects of climate change and the associated phenomena such as the forest fire on the stability of permafrost slopes.

The slope is assumed to have the same dimensions, soil properties, and initial conditions as that analyzed by the simplified Bishop method. The phase-coded image of the frozen slope is generated with MATLAB based on the soil physical constituents and properties of individual phases. The image is then converted into COMSOL and the corresponding physical, thermal, and mechanical properties of each phase (Table 2) are assigned based on the phase coding. For the thermal boundary conditions, thermal insulations are applied on the right side and the bottom of the slope. The initial temperature of the study region is assumed to be − 15 °C. For the mechanical boundary conditions, the fixed constraints are applied at the bottom of the slope and roller constraints are applied on the right side of the slope. The advantage of FEM model with COMSOL is that the thermomechanical coupling is automatically enabled by the thermal and mechanical

parameters of the soil constituents. When the temperature of a particular soil element is under or equal to 0° C, phase transition is assumed to occur. Due to the complexity in directly applying phase transition, the latent heat is applied as equivalent heat capacity over a small temperature transition zone. Upon phase transition from frozen to unfrozen condition, the corresponding thermo and mechanical properties of the phase are changed from ice to water, and the strength parameters of the soil are changed from those of frozen to unfrozen soils.

To study the effects of climate conditions on the stability of the slope, the daily average temperature in 1956 and 2017[1], respectively, and the predicted monthly average temperature in 2045[2], at Anchorage, Alaska (Fig. 7), are applied on top of the slope surface. A few locations were selected to examine the process occurring in the slope. Figure 8 shows the computational domains with FEM mesh and positions of 4 probes. The probes define sample locations and are used to describe how temperature as well as LFS varied with time at the given position.

The computational simulations are conducted on the responses of the slope over the whole year (365 days) period. Examples of simulation results are summarized in Figs. 9, 10, 11, and 12. The results show that from March 1, 1956, to July 1, 1956, the temperature on the slope surface rises from − 6.17 to 15.8° C and the corresponding thawing depth keeps penetrating below the slope surface (Fig. 9). The shear strength decreases in the melting soil elements where the temperature rises above 0° C. The local factor
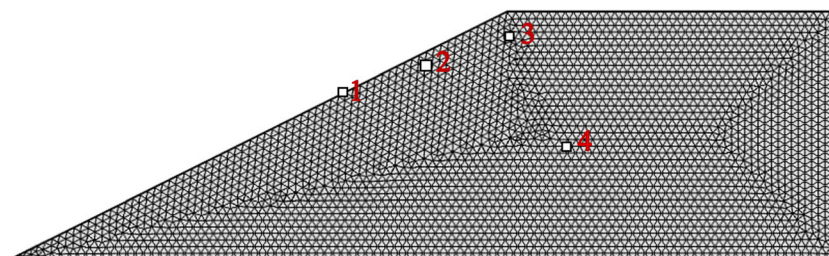
Fig. 8 Computational domains of the slope with FEM mesh and probe locations where simulation results are monitored (i.e., 1, 2, 3, 4)
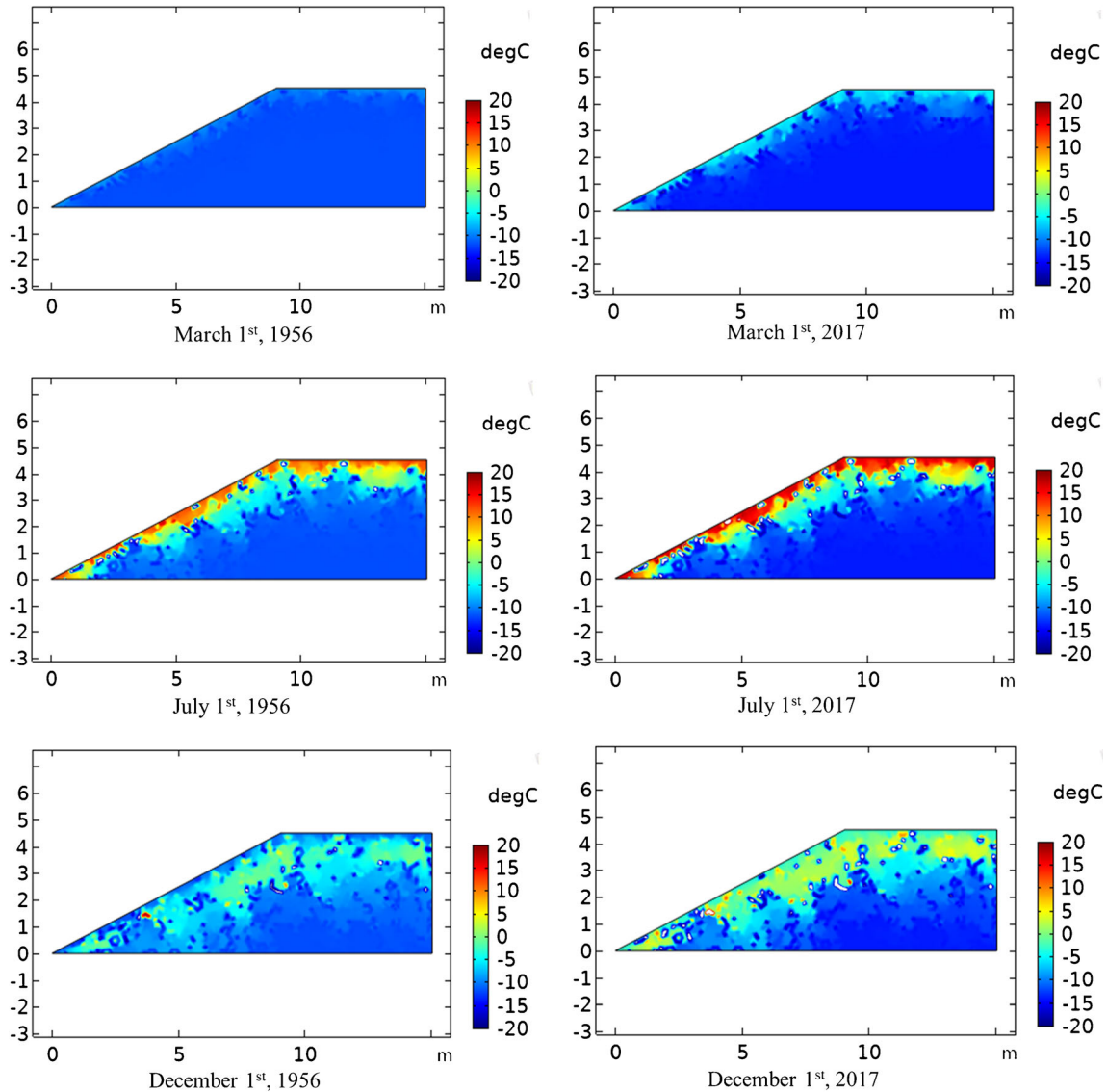
Fig. 9 Comparison of the temperature distribution in the slope during the freezing/thawing process in 1956 and 2017

of safety drops below 1 indicating failure in the corresponding soil element (Fig. 10). The failure of the slope keeps evolving with the penetration of thawing front. The failure surface of the slope is parallel to the thawing front and generally parallel to the slope surface. This phenomenon agrees with the field observation (Davies et al. 2001). It should be noted that the contour plot of the LFS and thaw depth penetration lines are not uniformly distributed due to the microstructure of the soil. The overall distribution patterns, however, are generally parallel to the slope surface.

From July 1, 1956, to December 1, 1956, as the season transition to the freezing season, the temperature on the slope surface drops from 15.8 to 1.2° C (Fig. 9) and the previous thawed soil in the slope refreezes during this period. The shear strength increases in the soil where the temperature drops below 0° C. This increases the local factor of safety above 1, which prevents the slope from further moving (Fig. 10).

With the impact of climate change, the average temperature increases from 1956 to 2017. For example, compared between July 1, 1956, and July 1, 2017, the surface temperature of the slope increases from 15.8 to 19.7° C. The thawing depth is deeper on July 1, 2017, than that of the thawing depth on July 1, 1956 (Fig. 9). The area in the slope with local factor safety smaller than 1 indicates failure and is defined as $S_{LFS<1}$. By exporting the point data of LFS distribution graphs in COMSOL, the $S_{LFS<1}$ is calculated as the summation of point taken area with LFS < 1. As shown in Fig. 10, $S_{LFS<1}$ is 10.47 m² on July 1, 2017, which is 20% larger than that of 8.19 m² on July 1, 1956. Overall, the slope is less stable in 2017 than that of 1956 due to climate change.

To further predict the effects of climate change on the stability of the thawing slope, the forecasted temperature process in 2045 is applied to the initial frozen slope. The corresponding local factor of safety distribution in the slope is calculated and is shown in Fig. 11. Compared with March 1, 2017, on March 1, 2045, the failure area
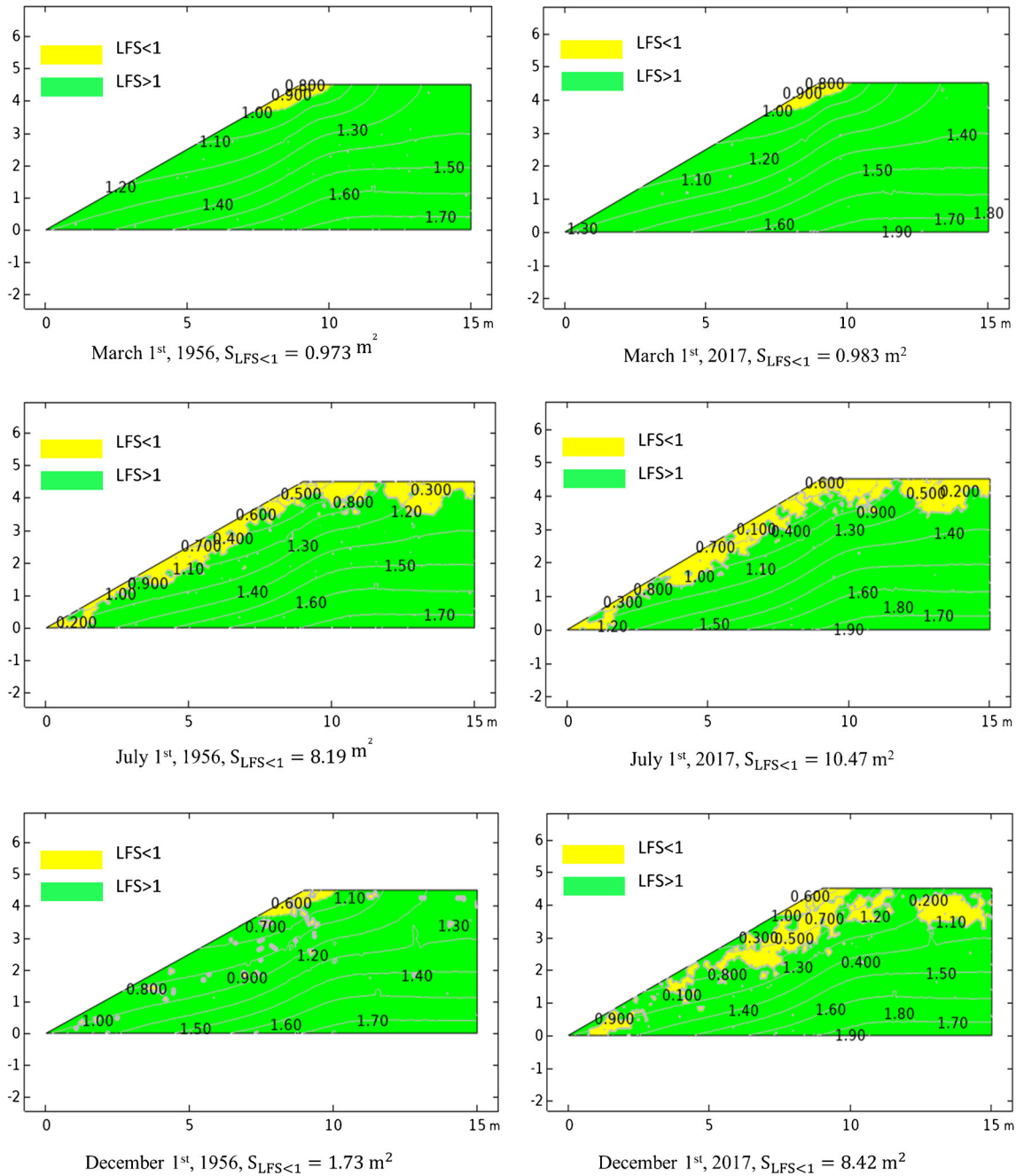
Fig. 10 Comparison of the local factor of safety distribution in the slope during the thawing/freezing process in 1956 and 2017

along the slope increases from 0.983 to 2.96 m² (over 190%) and from July 1, 2017, to July 1, 2045, the failure area of the slope increases from 10.47 to 11.34 m² (over 8%). This clearly demonstrates that the frozen slope is likely to subject to more instability issues due to climate change.

The local factor of safety is not only a function of position but also a function of time and temperature. Figure 12 shows the variations of local factor of safety at four probe locations (Fig. 8) inside the slope in 2017. One of the location (probe no. 3) is located in area subjected to freezing/thawing processes. The other location (probe no. 4) is located in area that is not subjected to freezing/thawing processes (or permafrost). For probe no. 3, the local factor

of safety is above 1 when the temperature is below 0 °C, while it is below 1 when the temperature is above 0 °C. This is partially due to the significant transition of soil strength under freezing or thawing conditions. While for location 4, which is further inside the slope and not subjected to freezing/thawing transition, the local factor of safety maintains relative stable. The minor change is primarily due to the change of internal stress field associated with freezing/thawing process along the slope.

### Effects of burning on slope stability in the cold regions

There is increasing occurrence of natural hazards such as forest fire observed in the cold regions. The RFEM model provides an
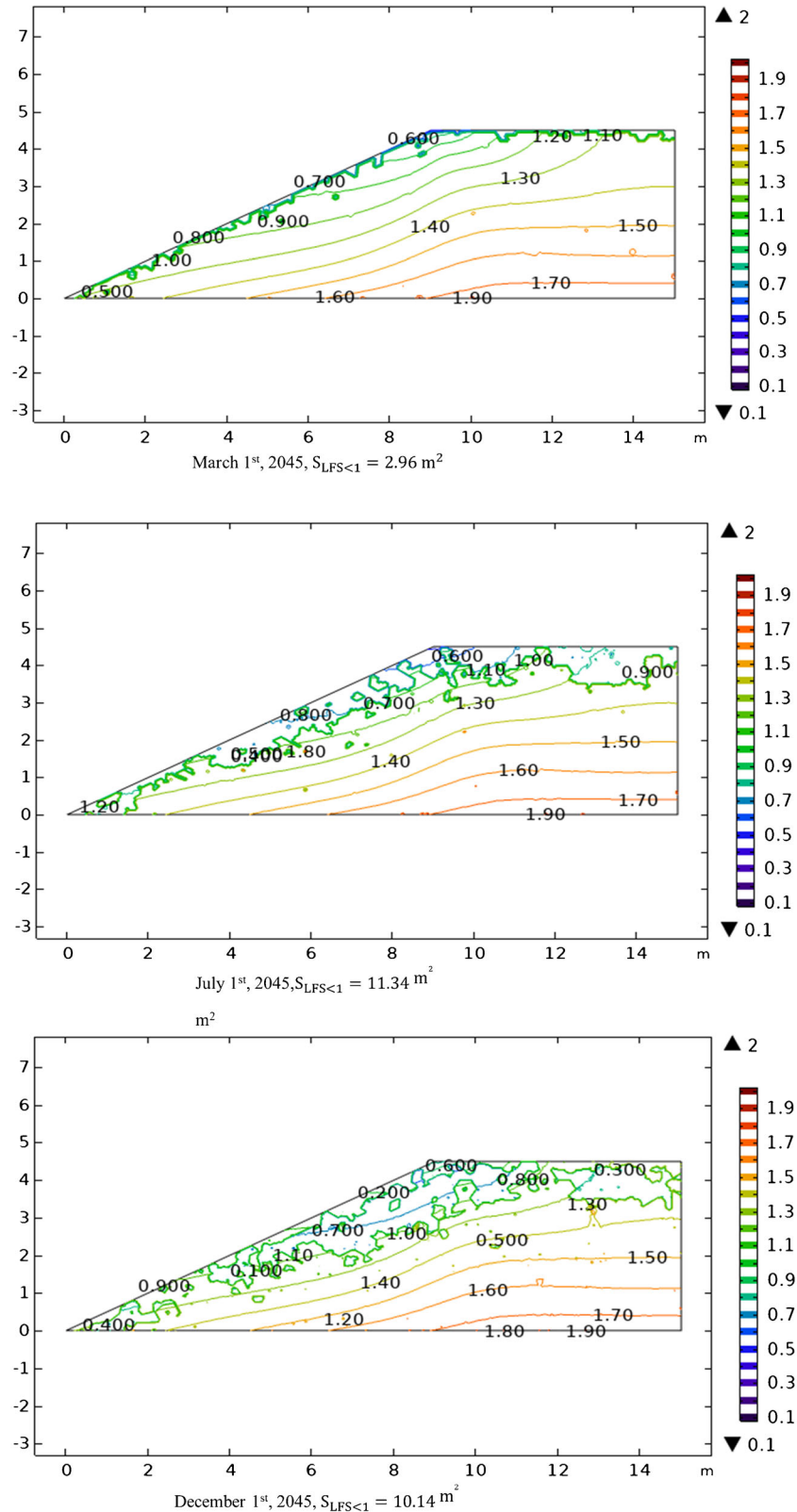
Fig. 11 The local factor of safety distribution along the slope based on forecasted climate process in 2045

effective tool to investigate the impacts of transient thermal process on the stability of cold region slope. The same slope is used as the analyses testbed. For the thermal boundary conditions, thermal insulations are applied on the right side and the bottom boundary of the slope. The initial temperature of the slope is assumed to be − 15 °C. For the mechanical boundary conditions,

Probe No. 1

Probe No. 2

Probe No. 3

Probe No. 4
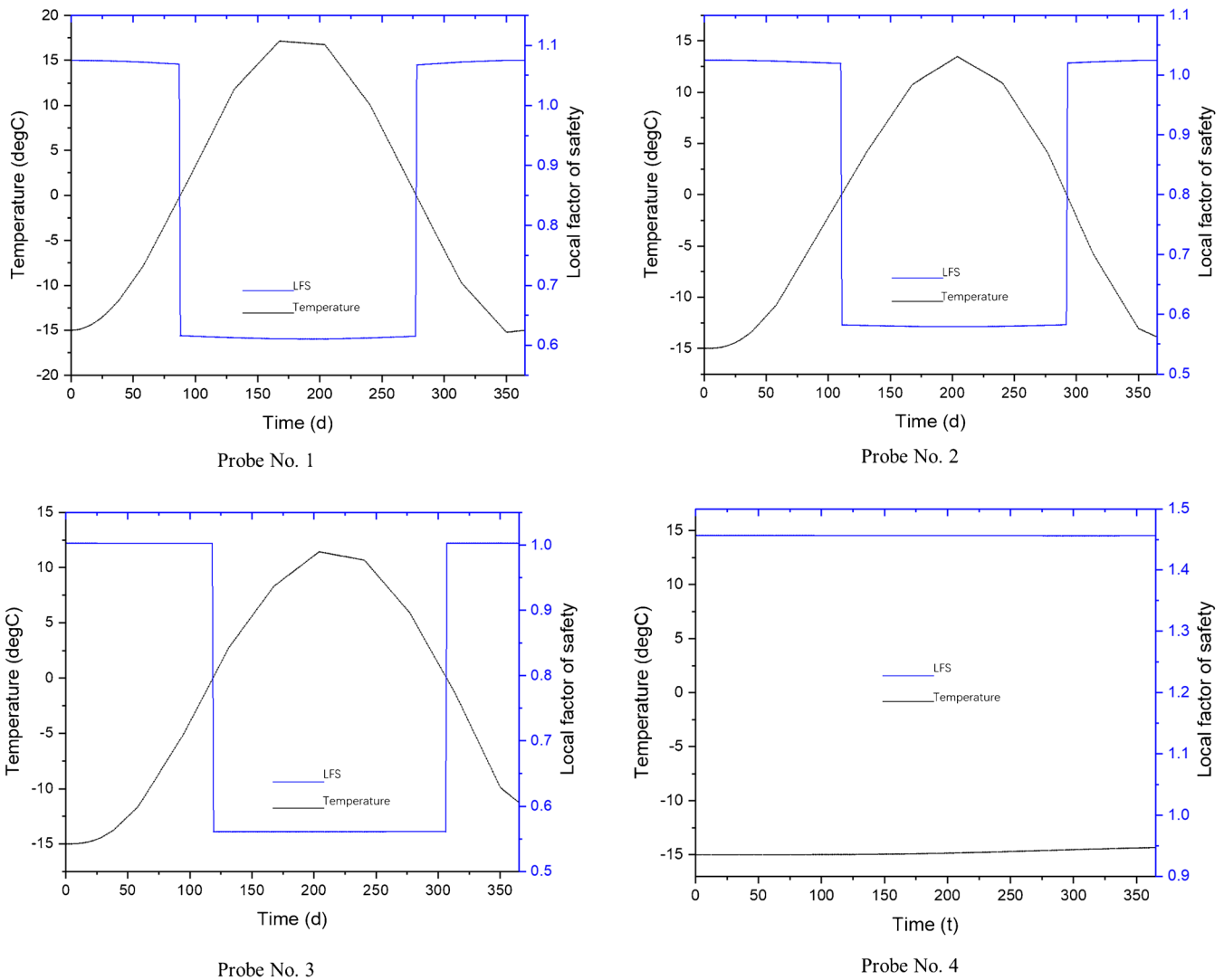
Fig. 12 Temperature and local factor of safety at different locations (corresponding to probe locations defined in Fig. 8) on the slope during the thawing/freezing process

the fixed constraints are applied to the bottom of the slope and roller constraints are applied to the right side of the slope.

It is assumed that half area on the slope is burned in a forest fire (Fig. 13) where the experimentally measured temperature process in the topsoil is applied as the boundary condition to emulate the effects of burning (Fig. 14).

The RFEM simulation is conducted for the slope subjected to burning over 2-h period. The simulation results are summarized in Figs. 15 and 16 at locations along the horizontal and vertical directions.

Figure 15 illustrates the temperature process at different horizontal locations inside the slope. As shown in the figure, the temperatures at each location increase initially. After that, the temperature starts to decrease until reaching a steady state. For locations deeper into the slope surface, the temperature of the corresponding locations is less affected.

Figure 16 shows the local factor of safety contour calculated by RFEM during the burning process. When subjected to burning, the temperature in the frozen soil around the burning area rises which causes melting of the frozen soil. The local factor of safety drops
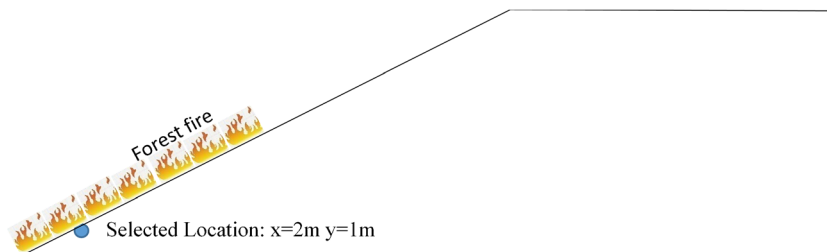
Fig. 13 Illustration of the slope and the area subjected to fire burning
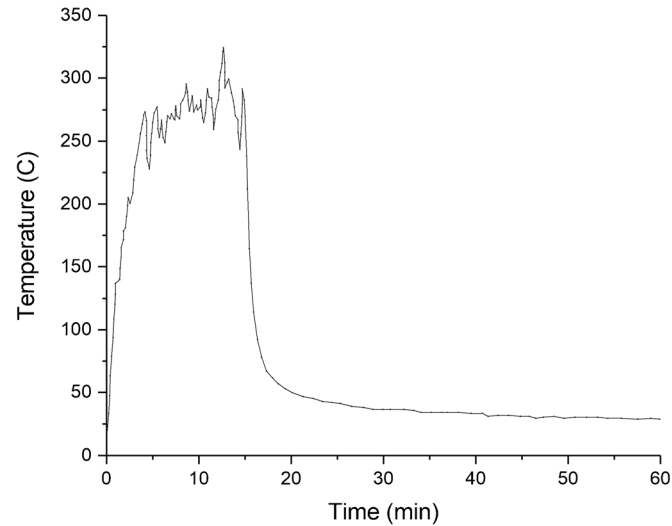
Fig. 14 Monitored temperature process on the surface of a burned mollic topsoil (soil was burned in a combustion tunnel by applying a flame with a blowtorch, (Badía et al. 2017)

below 1 in areas close to the toe of the slope, which would trigger localized failures. The failure surface along the slope is generally parallel to the slope surface and it is about 15 cm deep the maximum into the slope surface.

The overall observation from the results indicated that forest fire along a permafrost slope, with a duration of around 15 min, will mostly only affect the temperature field distribution in shallow depth along the slope. Consequently, it might trigger shallow failures along the slope, possibly in the form of shallow landslides. The weakened soil structure might also be inductive to process such as surface erosion which could further compromise the stability of the slope.

Discussions

The random finite element (RFEM) method developed in this paper applies phase coding to represent the soil constituent phases. The spatial-dependent material properties are assigned based on phase coding during the RFEM simulations. This presents a convenient way to describe the soil behaviors considering the constituents as well as the spatial distribution of soil phases, particularly under the condition that the fabric of individual particle does not affect its macroscopic behaviors. These include the situation when the soil grain is sufficiently small or the scale of geostructure is sufficiently large. Properties of individual phases can be determined by calibration with the results of physical experiments on the bulk soil samples. This RFEM combines the advantages of discrete element method (DEM) in describing the soil microstructure and constituents, as well as the advantages of finite element method (FEM) in efficient solving of the governing equations. Besides, the RFEM model allows capturing the multiphysics coupling processes (such as thermo-hydro-mechanical coupling) in soils with easiness.

The RFEM method is applied to analyze the slope stability of permafrost slopes subjected to climate effects (i.e., changing climates and forest fire). The localized factor of safety was used to identify the failure zones along the slope. With the combination of
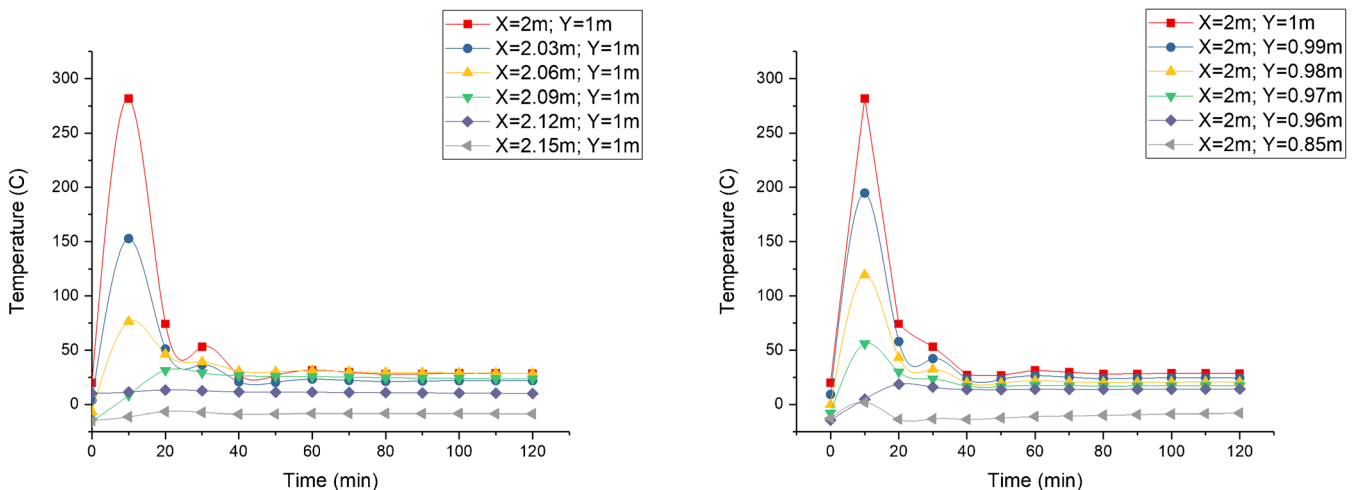
Fig. 15 Temperature behavior at different positions in the slope
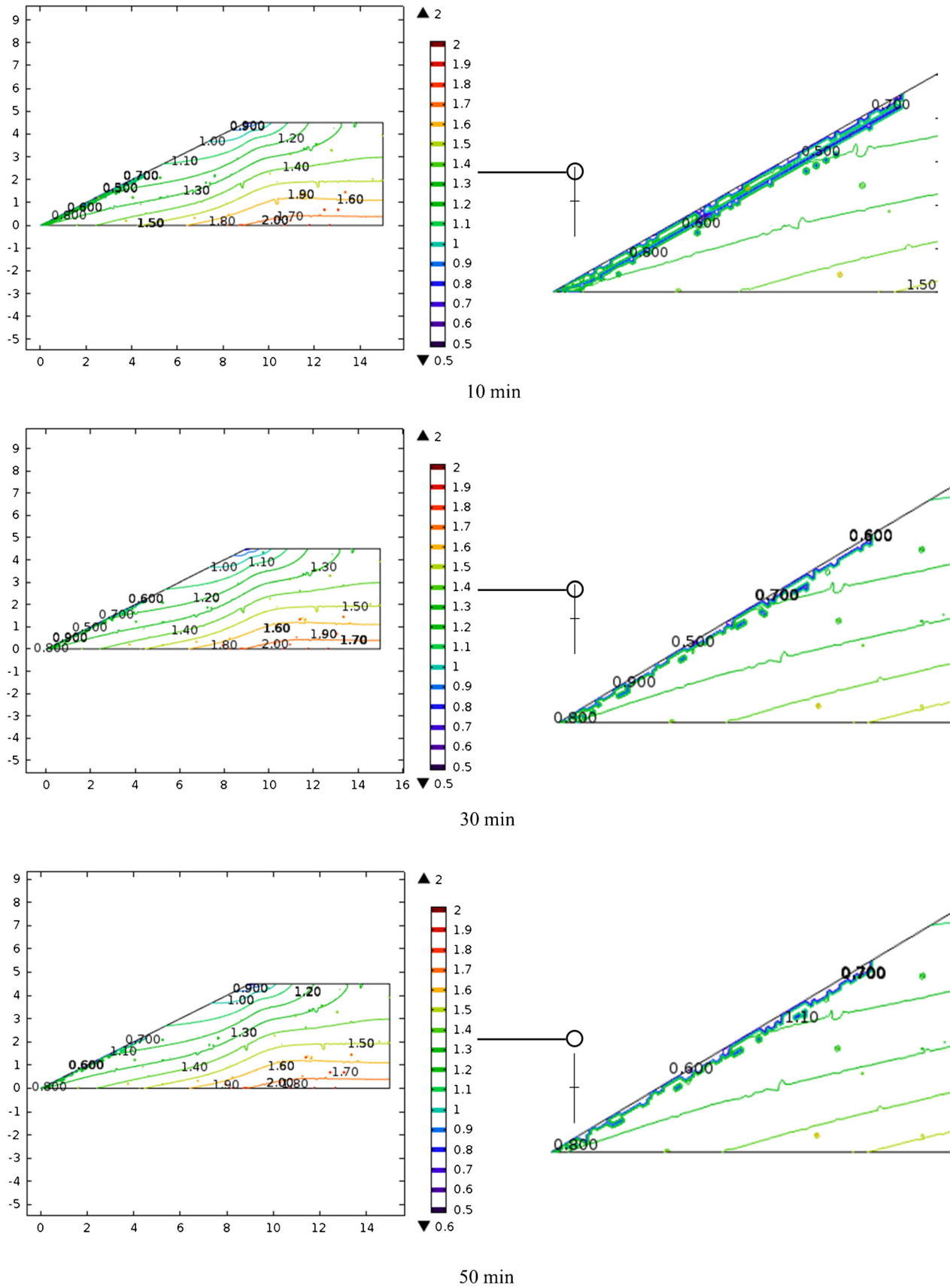
Fig. 16 Burning effects on the local factor of safety of the slope

RFEM and local factor of safety, the failure zones of the permafrost slope subjected to different climate change scenarios were analyzed. The results showed that the changing climates have a major influence on the slope failures due to thawing effects. The effects of forest fire along the slope were also analyzed, which indicates that the melting of permafrost slope due to surface fire will lead to shallow slides along the slope. Overall, the microstructure-based RFEM is an effective modelling approach to simulate the effects of thermomechanical coupling on slope stability for cold region slopes.

Conclusion

A novel microstructure-based random finite element (RFEM) model is developed to analyze the stability of cold region slope subjected to thawing due to climate change and localized burning by forest fire. Compared with commonly used global stability analyses by limit equilibrium method, this model considers the temperature variations associated with the freezing/thawing processes and its impacts on soil mechanical strengths. The phase-coded RFEM models for soils are firstly built to simulate the bulk behaviors of both frozen and unfrozen soils. The experimental results of uniaxial compression test on unfrozen or frozen soil specimens are compared with RFEM simulation results to calibrate the parameters for soil phases. Subsequently, the shear strength parameters, i.e., the cohesion and angle of internal friction, of unfrozen and frozen soils were then obtained from simulated triaxial tests using the RFEM model. Slope stability analyses are conducted with the RFEM model considering coupled thermomechanical fields subjected to climate processes. The simulation results show that the predicted failure behaviors are consistent with slump failure commonly observed in cold region slopes. Besides, the stability of cold region slopes varies with time over a year and is affected by the climate change. Transient events such as forest fire primarily cause localized failure along the slope. This new RFEM method provides a novel approach to analyze the stability of cold region slopes subjected to various thermal processes.

References

Alley RB, Marotzke J, Nordhaus WD, Overpeck JT, Peteet DM, Pielke RA et al (2003) Abrupt climate change. Science 299(5615):2005–2010

Arenson LU, Springman SM (2005) Triaxial constant stress and constant strain rate tests on ice-rich permafrost samples. Can Geotech J 42(2):412–430

Badía D, López-García S, Martí C, Ortíz-Perpiñá O, Girona-García A, Casanova-Gascón J (2017) Burn effects on soil properties associated to heat transfer under contrasting moisture content. Sci Total Environ 601:1119–1128

Bishop AW (1955) The use of the slip circle in the stability analyses of slopes. Geotechnique 5(1):7–17

Bo MW, Fabius M, & Fabius K (2008) Impact of global warming on stability of natural slopes. In Proceedings of the 4th Canadian Conference on Geohazards: From Causes to Management, Presse de Univ. Laval, Quebec.

Chamberlain E, Groves C, Perham R (1972) The mechanical behavior of frozen earth materials under high pressure triaxial test conditions. Geotechnique 22(3):469–483

Czurda KA, Hohmann M (1997) Freezing effect on shear strength of clayey soils. Appl Clay Sci 12(1-2):165–187

Davies MC, Hamza O, Harris C (2001) The effect of rise in mean annual temperature on the stability of rock slopes containing ice-filled discontinuities. Permafr Periglac Process 12(1):137–144

Dong S, Yu X (2016) Experimental characterization and microstructure based random FEM simulation of freezing and thawing effects on soils. Geotechnical Special Publication:711–719

Dong S, Yu X (2017) Microstructure-based random finite element simulation of thermal and hydraulic conduction processes in unsaturated frozen Soils. Geotechnical Special Publication:781–790

Dong S, Yu XA (2018) Microstructure-based finite element model to estimate hydraulic properties in fine-grained soils. Geotechnical Special Publication:258–265

Duncan JM (1996) State of the art: limit equilibrium and finite-element analyses of slopes. J Geotech Eng 122(7):577–596

Fenton GA, Griffiths DV (2003) Bearing capacity prediction of spatially random c-φ soils. Can Geotech J 40(1):54–65

Fenton GA, Griffiths DV, Williams MB (2005) Reliability of traditional retaining wall design. Geotechique 55(1):55–62

Frauenfeld OW, Zhang T, Mccreight JL (2007) Northern hemisphere freezing/thawing index variations over the twentieth century. Int J Climatol 27(1):47–63

Griffiths DV, Fenton GA, Manoharan N (2006) Undrained bearing capacity of two-strip footings on spatially random soil. Int J Geomech 6(6):421–427

Griffiths DV, Huang J, Fenton GA (2010) Probabilistic infinite slope analyses. Comput Geotech 38(4):577–584

Gruber S, & Haeberli W (2007) Permafrost in steep bedrock slopes and its temperature-related destabilization following climate change. J Geophys Res Earth Surf 112(F2).

Gruber S, Hoelzle M, Haeberli W (2004) Permafrost thaw and destabilization of Alpine rock walls in the hot summer of 2003. Geophys Res Lett:31(13)

Haeberli W, Beniston M (1998) Climate change and its impacts on glaciers and permafrost in the Alps. Ambio:258–265

Harris C, Davies MC, Etzelmüller B (2001) The assessment of potential geotechnical hazards associated with mountain permafrost in a warming global climate. Permafr Periglac Process 12(1):145–156

Hivon EG, Sego DC (1995) Strength of frozen saline soils. Can Geotech J 32(2):336–354

Janbu N (1973) Slope stability computations. Publication of, Wiley (John) and Sons, Incorporated

Jorgenson MT, Racine CH, Walters JC, Osterkamp TE (2001) Permafrost degradation and ecological changes associated with a warming climate in central Alaska. Clim Chang 48(4):551–579

Kim JW, Lu Z, Qu F, Hu X (2015) Pre-2014 mudslides at Oso revealed by InSAR and multi-source DEM analyses. Geomatics, Natural Hazards and Risk 6(3):184–194

Lu N, Şener-Kaya B, Wayllace A, Godt JW (2012) Analyses of rainfall-induced slope instability using a field of local factor of safety. Water Resour Res 48(9)

Luo J, Niu F, Lin Z, Liu M, Yin G (2019) Recent acceleration of thaw slumping in permafrost terrain of Qinghai-Tibet Plateau: an example from the Beiluhe Region. Geomorphology 341:79–85

McRoberts EC, Morgenstern NR (1974) The stability of thawing slopes. Can Geotech J 11(4):447–469

Morgenstern NU, Price VE (1965) The analyses of the stability of general slip surfaces. Geotechnique 15(1):79–93

Niu F, Luo J, Lin Z, Fang J, Liu M (2016) Thaw-induced slope failures and stability analyses in permafrost regions of the Qinghai-Tibet Plateau, China. Landslides 13(1):55–65

Nixon JF, Lem G (1984) Creep and strength testing of frozen saline fine-grained soils. Can Geotech J 21(3):518–529

Shaoling W, Huijun J, Shuxun L, Lin Z (2000) Permafrost degradation on the Qinghai-Tibet Plateau and its environmental impacts. Permafr Periglac Process 11(1):43–53

Sturm M, Racine C, Tape K (2001) Climate change: increasing shrub abundance in the Arctic. Nature 411(6837):546–547

Thibault S, Payette S (2009) Recent permafrost degradation in bogs of the James Bay area, northern Quebec, Canada. Permafr Periglac Process 20(4):383–389

Wang DY, Ma W, Niu YH, Chang XX, Wen Z (2007) Effects of cyclic freezing and thawing on mechanical properties of Qinghai-Tibet clay. Cold Reg Sci Technol 48(1):34–43

Wang H, Xing X, Li T, Qin Z, & Yang J (2014) Slope instability phenomenon in the permafrost region along the Qinghai-Tibetan highway, China. *In Landslides in Cold Regions in the Context of Climate Change*. Springer, Cham, pp. 11-22.

Wu TH (1984) Soil movements on permafrost slopes near Fairbanks, Alaska. Can Geotech J 21(4):699–709

Zwiers FW (2002) Climate change: the 20-year forecast. Nature 416(6882):690–691

S. Dong · Y. Jiang
Department of Civil and Environmental Engineering,
Case Western Reserve University,
Cleveland, USA

S. Dong
e-mail: sxd405@case.edu

Y. Jiang
e-mail: yxj470@case.edu

X. Yu (✉)
Opal J. and Richard A, Vanderhoof Professor and Chair, Department of Civil and Environmental Engineering,
Case Western Reserve University,
Cleveland, USA
Email: xiong.yu@case.edu